Local Magnitude Discrepancies for Near-Event Receivers: Implications for the U.K. Traffic-Light Scheme

by Antony Butcher, Richard Luckett, James P. Verdon, J.-Michael Kendall, Brian Baptie, and James Wookey

Abstract Local seismic magnitudes provide a practical and efficient scale for the implementation of regulation designed to manage the risk of induced seismicity, such as Traffic-Light Schemes (TLS). We demonstrate that significant magnitude discrepancies (up to a unit higher) occur between seismic events recorded on nearby stations (< 5 km) compared with those at greater distances. This is due to the influence of sedimentary layers, which are generally lower in velocity and more attenuating than the underlying crystalline basement rocks, and requires a change in the attenuation term of the M_L scale. This has a significant impact on the United Kingdom's (U.K.) hydraulic fracturing TLS, whose red light is set at M_L 0.5. Because the nominal detectability of the U.K. network is M_L 2, this scheme will require the deployment of monitoring stations in close proximity to well sites. Using data collected from mining events near New Ollerton, Nottinghamshire, we illustrate the effects that proximity has on travel path velocities and attenuation, then perform a damped least-squares inversion to determine appropriate constants within the M_L scale. We show that the attenuation term needs to increase from 0.00183 to 0.0514 and demonstrate that this higher value is representative of a ray path within a slower more attenuating sedimentary layer compared with the continental crust. We therefore recommend that the magnitude scale $M_L = \log(A) + 1.17\log(r) + 0.0514r - 3.0$ should be used when local monitoring networks are within 5 km of the event epicenters.

Introduction

Any subsurface activity that alters the state of stress in the ground is capable of triggering seismic activity on pre-existing faults. In the United Kingdom (U.K.), coal mining has long been the dominant cause of these anthropogenic events (Wilson *et al.*, 2015). However, with the coal industry in decline, concerns about induced seismicity have switched to the nascent shale gas industry.

In response to these concerns, the U.K.'s Oil and Gas Authority has imposed a Traffic-Light Scheme (TLS) to manage induced seismicity, with an amber warning set at a local magnitude (M_L) of 0.0, and a red light at M_L 0.5, in which injection must cease followed by a 24-hr monitoring period (Department of Energy and Climate Change, 2015). A local magnitude scale is used, as opposed to other scales such as the moment magnitude, because the measurement is less complicated: the local magnitude scale is empirical, directly relating the measured maximum displacement amplitude (typically associated with the *S*-wave arrival) and hypocentral distance to M_L. For such a scheme to maintain the confidence of the industry, the regulators, and the general public, the local magnitude scale used to quantify event magnitudes must be robust and well constrained.

The existing U.K. local magnitude scale (Ottemöller and Sargeant, 2013) was calibrated using larger events, most of which were recorded at considerable distance (> 50 km) from their epicenters. Out of necessity, the TLS will be monitored by local networks within 5 km of the epicenters of any events that may occur. In this article, we seek to highlight issues with the local magnitude scale when used on shallow events located in close proximity to the receivers.

In April 2011, hydraulic fracturing operations at the Preese Hall well, near Blackpool, U.K., caused an M_L 2.3 earthquake (Clarke *et al.*, 2014). This event was felt by local people, causing considerable public concern despite its relatively small magnitude. In response, the British Geological Survey (BGS) installed temporary seismic stations close to the epicenter and recorded several subsequent, smaller events during further hydraulic fracturing stages.

As the first recorded instance of seismicity induced by hydraulic fracturing in the U.K., these events have been the subject of much interest (e.g., O'Toole *et al.*, 2013; Westaway, 2016). One aspect of the data that was immediately apparent was the discrepancy in local magnitude. Ground motions measured using a local monitoring station located
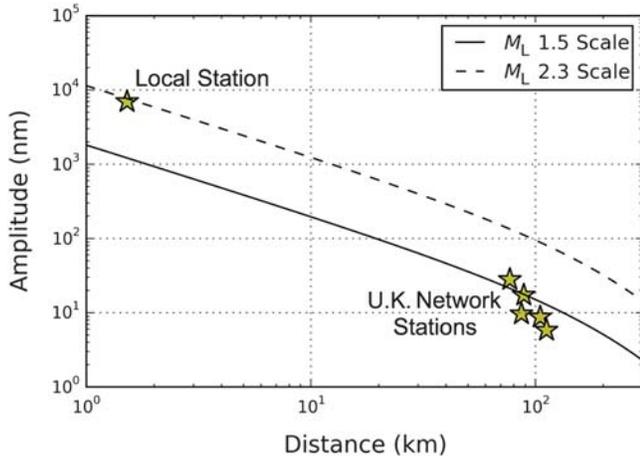
Figure 1. Measured ground displacements for the largest event at Preese Hall to be recorded by both local and distant stations (yellow stars). The expected displacements for M_L 1.5 and 2.3 events are shown by the solid and dashed lines, respectively. These measurements show the discrepancies in ground motion between a locally installed seismic station and the more distant United Kingdom (U.K.) seismic network.

at hypocentral distances of 1.5 km differed significantly in comparison with those calculated using the national U.K. seismic monitoring network, the nearest station of which was at a distance of ∼80 km.

Based on the existing local magnitude scale, the largest event recorded by both distant and local stations had a magnitude of M_L 1.5 calculated on the national network, but M_L 2.3 on a local station located at an epicentral distance of 1.5 km (Fig. 1). Because of this discrepancy, magnitudes of events observed on only the Preese Hall network were assigned though scaling relative to a master event using the equation

$$M_{\text{DetectEvent}} = M_{\text{MasterEvent}} + \log\left(\frac{A_{\text{DetectEvent}}}{A_{\text{MasterEvent}}}\right), \quad (1)$$

in which A is the maximum amplitude measured on the waveform and M is the magnitude of the master or detected event (Eisner *et al.*, 2011).

The BGS seismic catalog shows several other examples of magnitude discrepancies for events in close proximity to receivers, and several studies have also identified either overestimation in magnitudes or larger than predicted amplitudes at close distances in other settings (Scognamiglio *et al.*, 2012; Atkinson *et al.*, 2014). A common explanation for these discrepancies is that nearby stations may be more impacted by event location errors. However, in Figure 2, we show the impact of a 0.5 km location error: although nearby stations are more impacted, the resulting magnitude error is insufficient to account for the discrepancies observed at Preese Hall. Moreover, if event location errors, or local site effects, were causing magnitude errors, we would expect these discrepancies to be random in nature, leading to both under- and overestimates of event magnitudes. Instead, we
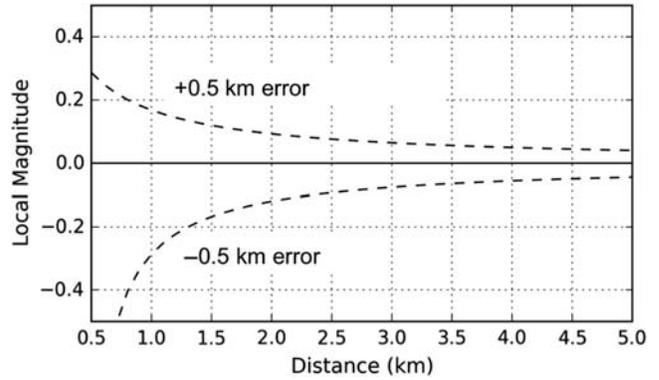
Figure 2. Impact of introducing a positional error of 0.5 km on calculated magnitudes. At a distance of 1.5 km, comparable with Preese Hall, the maximum magnitude discrepancy is no more than 0.2 units.

tend to see only overestimation of magnitudes at close distances: a systematic error implying a methodological issue with the use of local magnitude scales.

Local Magnitude (M_L)

The Richter equation for M_L is defined as

$$M_L = \log(A_{\text{WA}}) - \log(A_0), \quad (2)$$

in which A_{WA} is zero-to-peak amplitude measured on a standard horizontal Wood–Anderson seismograph, and $-\log(A_0)$ is the displacement correction term (Shearer, 2009). The displacement correction term accounts for geometrical spreading and attenuation, and calibrates the scale to Richter's original definition. In equation (2), the displacement amplitude is given in millimeters and gain corrected to a Wood–Anderson seismograph. Often M_L scales remove the gain correction and change units to nanometer using the term

$$\log(A_{\text{WA}}) = \log(A) + \log\left(\frac{2080}{10^6}\right). \quad (3)$$

Ottemöller and Sargeant (2013) developed the most recent M_L scale for the U.K., replacing the original scale of Hutton and Boore (1987) that was derived for southern California. The inversion of 1482 observations from 85 earthquakes on 50 stations anchored to a reference distance of 100 km led to the following local magnitude scale:

$$M_L = \log(A) + 0.95 \log(r) + 0.00183r - 1.76, \quad (4)$$

in which A is the horizontal-component ground displacement amplitude filtered with Wood–Anderson response in nanometers and r is the hypocentral distance in kilometers. Because observations were taken from earthquakes recorded on the U.K. network, the dataset used by Ottemöller and Sargeant (2013) is dominated by events with magnitudes larger than M_L 2.0 with epicentral distances > 50 km. As a result,

the current U.K. M_L scale has not been well calibrated for small-magnitude, near-receiver events, such as those recorded at Preese Hall, or potentially at future shale gas extraction sites.

For a local earthquake, the S-wave amplitude A can be expressed as a function of hypocentral distance r by

$$A(r) = A_0 r^{-\beta} e^{\frac{-\pi f r}{vQ}}, \tag{5}$$

in which A_0 is the initial amplitude, β is the geometrical spreading, f is the frequency, v is the path averaged S-wave velocity, and Q is the quality factor, which is inversely proportional to the anelastic attenuation. Havskov and Ottemoller (2010) show that taking the logarithm of equation (5) produces

$$\log(A(r)) = -\beta \log(r) - 0.43 \frac{-\pi f r}{vQ} + \log(A_0). \tag{6}$$

If f, v, and Q are assumed to be constant, the displacement correction term can be expressed in the form

$$-\log(A_0) = a \log(r) + br + c, \tag{7}$$

in which a, b, and c are constants representing geometrical spreading, attenuation, and the base level, respectively. Two different anchor points are commonly used to link the M_L scale to Richter's definition. Originally, a magnitude 3.0 earthquake was defined as a 1 mm displacement at 100 km, and more recently a 10 mm displacement at 17 km has been used to adjust the scale to other regions with significantly different attenuation (Hutton and Boore, 1987). Anchoring the displacement correction term to 17 km results in the equation

$$-\log(A_0) = a \log(r/17) + b(r - 17) + 2. \tag{8}$$

It can be seen that because the geometrical spreading does not vary significantly from 1, the greatest impact on the M_L scale will be caused by changes to the attenuation term b and its subsequent effect on the base level constant c. From equations (6) and (7), b can be represented by the equation

$$b \approx 0.43 \frac{\pi f}{vQ}, \tag{9}$$

and considering equations (3) and (8), the constant term c in equation (7) is derived using

$$c = 2 - a \log(17) + b(17) + \log(2080/10^6). \tag{10}$$

When considering shallow nearby events, we would expect a greater portion of the ray path to be through shallow sediments, as opposed to the more distant events used to calibrate the U.K.'s present M_L scale, which will have traveled predominantly through the deeper crust. We would therefore anticipate that both Q and v would be lower. Furthermore, because the path distance will be smaller, the frequency content f would likely be higher. These effects will have the combined effect of significantly increasing the attenuation constant b, which will have different impacts on the displace-
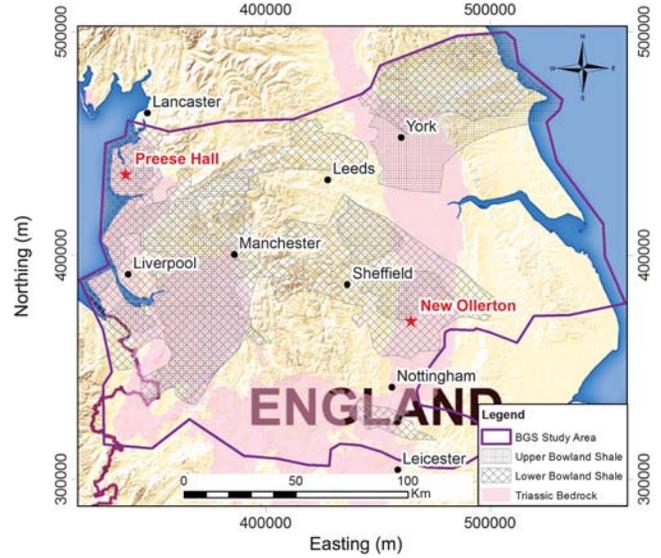
Figure 3. Location of Preese Hall and New Ollerton seismic events (red stars), along with the extent of lower and upper Bowland Shale units and Triassic bedrock.

ment equation (8) depending on the distance. At distances less than the anchor point, an increase in b will counterintuitively decrease the actual magnitude of the event, whereas at greater distances the magnitude will be increased. This can be seen by considering equations (8) and (10)—if r is less than 17, then an increase in b will result in a decrease in $-\log(A_0)$.

Data

To examine the impact that the proximity of receivers to seismic events has on M_L estimations, we use a series of seismic events recorded to the north of New Ollerton, Nottinghamshire, U.K. Although these events are not related to hydraulic fracturing, they do occur within the limits of the Bowland Shale as defined by the BGS, and comparable Triassic bedrock as the Preese Hall events (Fig. 3).

The New Ollerton area has a history of seismic activity relating to coal mining (Bishop *et al.*, 1993), and the locations and characteristics are consistent with coal seams worked by Thoresby Colliery, located ~800–900 m below the surface. The seams below this area are the Parkgate and Deep soft, and borehole records show that they are overlain by strata of sandstones, limestones, and marls (IMC Group Consulting Limited, 2003). Deep soft is the most recently operational seam, and was worked from 2010 until the closure of the colliery in July 2015. The coal was extracted using the longwall mining method, in which the roof is supported while a cutting machine is pulled along the width of the coal face. As the machine moves forward, the supports are advanced and the roof behind the supports is allowed to fall into the void left by the coal.

Between 5 February 2014 and 30 October 2014, a temporary network (here called NOL) was deployed by the BGS,
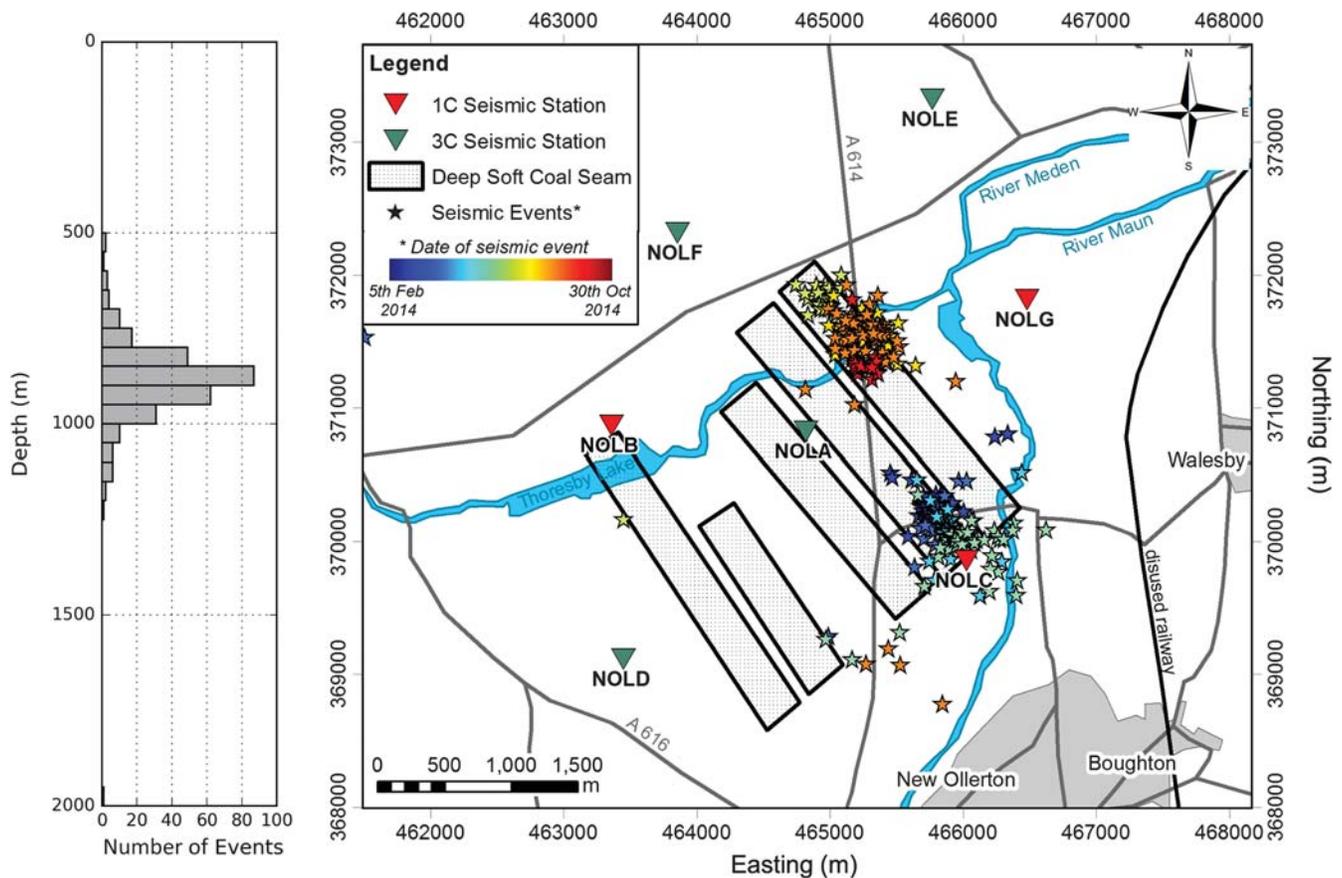
Figure 4. (Left) Depth distribution of seismic events. (Right) Location of New Ollerton network (inverted triangles), recorded seismic events (stars), and coal seam panels (black rectangles). Seismic events have been color coded to show temporal distribution. Position and depth distribution show a strong correlation with the excavated coal panels.

which comprises 4 three-component Güralp 3ESP broadband instruments (NOLA, NOLD, NOLE, and NOLF) and 3 vertical-component Geotech S13J instruments (NOLB, NOLC, and NOLG) with an aperture of about 5 km (Fig. 4). During the deployment, 296 events were recorded that fall within a source–receiver distance range of between 1 and 5 km. These events produced 2221 amplitude observations from the individual horizontal components of the three-component stations (Fig. 5).

Locations of seismic events were determined initially through the inversion of *P*- and *S*-wave travel-time picks using a 1D velocity model of Bishop *et al.* (1993) (Table 1). Event locations are plotted in Figure 4, and a strong correlation with the position and depth of the excavated coal panels is noted. It can be seen that events track mining operations, changing position over time, with two distinct clusters observed that relate to activity in different coal panels. We estimate location errors to be ∼100 m (95% confidence interval), and given their close match to the position of the deep soft coal panels, this implies an accurate velocity model. Therefore, considering Figure 2, errors in magnitude are not related to positional error.

Local magnitudes were initially calculated using displacement measurements made on the NOL network and the existing U.K. M_L scale using equation (4). Of these events, those with magnitudes $M_L > 1.7$ were also in general identifiable on the U.K. national seismic network after the application of a band-pass filter of 3–10 Hz. When applying the same filtering to the NOL stations, the same discrepancy observed at Preese Hall—an overestimate of M_L on nearby stations—is also present in this dataset (Fig. 6). This overestimate becomes larger as hypocentral distances are reduced.

Velocities and Attenuation

The velocity structure of the U.K. has been studied by numerous authors (e.g., Chadwick and Pharaoh, 1998; Kelly *et al.*, 2007; Davis *et al.*, 2012), with local *P*-wave crustal velocity structures derived from the Lithospheric Seismic Profile in Britain (Kelly *et al.*, 2007) and the Caledonian Suture Seismic Experiment (Bott *et al.*, 1985). Booth (2010) has also determined regional 1D velocity–depth models for the northern and central regions of the U.K., based on *P*-wave arrival from local earthquakes recorded between 1990 and 2008, which complement the refraction survey data. Understanding of the *S*-wave structure comes principally from the work in ambient noise Rayleigh-wave tomography
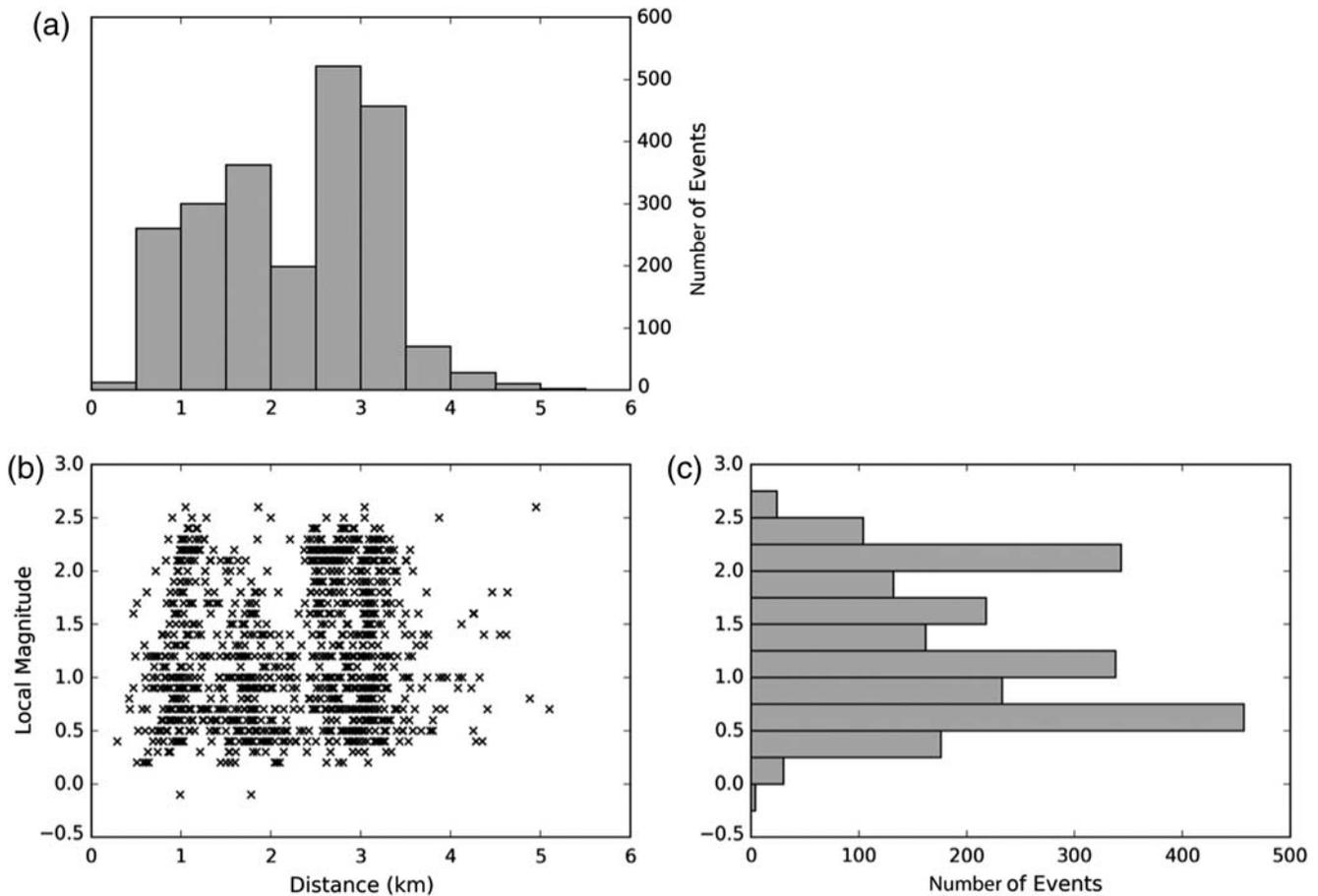
Figure 5. Distribution of hypocentral distances and local magnitudes for observations near New Ollerton. (b) Magnitude versus distance is presented along with the individual distribution of (a) distances and (c) magnitudes. Magnitudes are computed using the NOL network and the existing U.K. local magnitude scale.

(Nicolson *et al.*, 2014) and receiver functions (Tomlinson *et al.*, 2006; Davis *et al.*, 2012).

In general terms, the velocity structure in the U.K. comprises a highly variable sedimentary layer (Nicolson *et al.*, 2014), overlaying a faster continental basement, on top of a lower crust (Bott *et al.*, 1985) that extends to the Moho mapped at depths between 25 and 35 km (Chadwick and Pharaoh, 1998). Velocities within the sedimentary layer vary

Table 1
Seismic Velocity Structure for New Ollerton Area, from Bishop *et al.* (1993)

Depth (km)	V_P (km/s)	V_S (km/s)	Lithology
0–0.060	1.9	1.28	Weathered Sherwood sandstone
0.060–0.135	2.75	1.54	Unweathered Sherwood sandstone
0.135–0.275	3.1	1.74	Permian
0.275–1.019	3.5	1.97	Coal measures
1.019–2.751	5.2	2.92	Carboniferous limestone
2.751–37.751	6.0	3.37	?Precambrian

significantly depending on composition (see Table 2); for example, the *S*-wave velocity of sandstones is typically 1.5 km/s, with limestone higher at ∼3 km/s. Underlying the sedimentary layer, the continental crust comprises crystalline basement rocks, which typically have much higher velocities and can mark a sharp velocity discontinuity. Abercrombie (1997) has shown that anelastic attenuation, the inverse of Q, varies substantially between sedimentary and basement rocks. Within the sedimentary layer, Q is typically low (e.g., < 30), as demonstrated by Best *et al.* (2007), whereas in the crystalline basement rocks, Q increases by at least an order of magnitude (Abercrombie, 1995; Stork and Ito, 2004).

At New Ollerton, the sedimentary layer consists of a combination of sandstones, coal measures, gritstones, and limestones, which extend to a depth of ∼2.75 km where the continental basement is encountered (Bishop *et al.*, 1993). The velocity model produced by Bishop *et al.* (1993) was derived from borehole information, which extended to the coal measures, and deep seismic refraction data used to constrain the sedimentary continental crust boundary. Best *et al.* (2007) determined velocities, attenuation, and densities of

Figure 6. Displacement amplitude versus distance recorded on both the NOL network (stations < 5 km distance) and the U.K. national network (stations > 50 km distance) for two events (9 February 2014 05:33 and 12 February 2014 02:35 colored yellow and black, respectively). The U.K. scale for M_L 1.0, 2.0, and 3.0 (dotted, dashed, and solid lines) is also plotted. On the distant stations, the displacements match well with the U.K. scale for an M_L 1.0 event. On the nearby stations, displacements are substantially larger, and this discrepancy increases as hypocentral distance decreases.

multiple sandstone, limestone, and siltstone samples collected at depths ranging between 40 and 185 m from Whitchester, northeast England, using ultrasonic pulse-echo methods. Broadly classifying these results by lithology provides the range of velocities, attenuations, and densities shown in Table 2, which are comparable with the velocities observed at New Ollerton, and indicates the likely values of Q.

Impact of Hypocentral Distance

We demonstrate the impact that the sedimentary layer has on the path effects for near-event receivers using S-wave apparent velocities and estimates of Q. S waves are considered since their amplitudes are primarily used to derive M_L. Because the NOL dataset has limited observation within the 5–20 km range, events recorded within the general vicinity of New Ollerton are also included, which have been sourced from the BGS catalog.

In Figure 7, we show the apparent S-wave velocity (the epicentral distance divided by the travel time). A prominent knee occurs at a distance between 10 and 15 km, with V_{app} increasing as distance from the epicenter increases, which then stabilizes at a value of ~3.5 km/s at greater distances. These observations are modeled using a simple two-layer case, with a shallower layer representing sedimentary layers extending to a depth of 2.75 km with a velocity of 2.5 km/s, and a deeper layer comprising the continental basement with

a velocity of 3.6 km. Travel times (TT) are expressed using

$$\text{TT} = \frac{r}{v_{\text{base}}} + \frac{(2z_l - z_s)\cos\theta}{v_{\text{sed}}}, \qquad (11)$$

in which r is the epicentral distance, z_l is the layer depth, z_s is the source depth, v_{sed} and v_{base} are the average sedimentary and crustal layer velocities, respectively, and θ is the takeoff angle. The modeled apparent velocity (V_{app}) is therefore

$$v_{\text{app}} = \frac{r}{\text{TT}}, \qquad (12)$$

and it can be seen that the model provides a relatively good fit to the data (Fig. 7). This model demonstrates that the increase in velocity within the first 10–15 km relates to the decreasing contribution of the sedimentary layer on the ray path, with signals recorded at distances in excess of 10–15 km dominated by the faster less attenuating continental crust.

We calculate Q for eight events recorded on the same station (NOLF), with six near events occurring at a distance of ~2 km and a depth of 0.9 km, and two far events located at a distance of 60 km and a depth of 2.5 km. We use spectral methods to estimate the values of Q for both sets of events, through fitting a source model to the observed displacement spectra, generated using the multitapering technique developed by Prieto et al. (2009). Source spectra are modeled using the Brune (1970) model:

$$\Omega(f) = \frac{\Omega_0 e^{-(\pi ft/Q)}}{[1 + (f/f_c)^2]}, \qquad (13)$$

in which Ω_0 is the low-level frequency, f is the frequency, f_c is the corner frequency, and t is the travel time (following Prejean and Ellsworth, 2001; Stork et al., 2014). On each set of displacement spectra, we include source models generated using Q-values of 30, 300, and 600 (Fig. 8), and determine that the travel paths of near events have estimated Q_S of 30, whereas the distant events have estimated Q_S of 300. This illustrates that the wavepaths of the near events are traveling through different medium than the far events, with the $Q = 30$ traveling through the compared attenuating sedimentary layers and not the basement rocks.

The observations made at small epicentral distances will have significantly different attenuation effects than the distant observations used by Ottemöller and Sargeant (2013) to calibrate the U.K. M_L scale. Therefore, a corrected scale

Table 2
P- and *S*-Wave Velocities and Q from Laboratory Test, from Best et al. (2007)

Lithology	V_P (m/s)	V_S (m/s)	Q_P	Q_S	Density (kg/m³)
Sandstone	3266 ± 10 to 4807 ± 14	2140 ± 6 to 3076 ± 9	13 ± 1 to 88 ± 32	10 ± 1 to 61 ± 10	2491−2620
Limestone	5898 ± 18 to 6301 ± 9	3066 ± 9 to 3275 ± 10	22 ± 1 to 160 ± 88	17 ± 1 to 101 ± 27	2616−2661
Siltstone	3372 ± 10 to 4308 ± 13	2024 ± 6 to 2487 ± 7	18 ± 1 to 33 ± 1	10 ± 1 to 26 ± 3	2525−2637
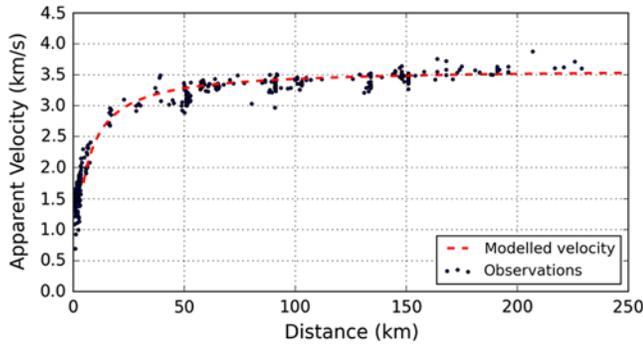
Figure 7. Apparent *S*-wave velocities from earthquakes within the U.K. Red dashed lines represent modeled apparent velocities for the simplified two-layer case, with shallow sedimentary layers of 2.5 km/s extending to a depth of 2.75 km, overlaying a continental basement with a velocity of 3.6 km/s.

must be developed if consistent magnitudes are to be calculated using stations deployed in close proximity to event epicenters.

M_L Scale Recalibration for Nearby Events Based on New Ollerton

Many studies have focused on verifying the southern California M_L scale originally developed by Richter (1935), or to recalibrate it for different regions to take into account different attenuation properties (e.g., Hutton and Boore, 1987; Langston *et al.*, 1998; Keir *et al.*, 2006; Ottemöller and Sargeant, 2013; Di Bona, 2016). The common approach is to invert observations using a least-squares method to determine the geometric spreading and attenuation terms, while also solving for magnitudes. Recent studies tend to anchor the displacement correction term to 17 km, because it is easier to adjust the scale to other regions with significantly different attenuation (Alsaker *et al.*, 1991). Although the New Ollerton observations are very localized, they occur within the area of the Bowland Shale, and we seek to invert them to gain an indication of the appropriate scale required for near-receiver events.

We use a Levenberg–Marquardt algorithm, which is a damped least-squares method, to determine the best-fitting geometrical spreading and attenuation terms at New Ollerton. Because of the limited distance range of the observations, attempts to determine these values while also treating the magnitudes as an unknown have failed to converge. Furthermore, our aim was to create a scale that remained consistent with the existing U.K. local magnitude scale, which has been well established for events recorded on more distant stations. Therefore, we instead determined the average magnitude discrepancies observed between the NOL network and the U.K. network, recalibrated magnitudes, and used these values to constrain the inversion. We determined the geometric spreading a and attenuation b terms for observed amplitudes A_{ijk} magnitudes M_{Lik} and distances r_{ij} using the model
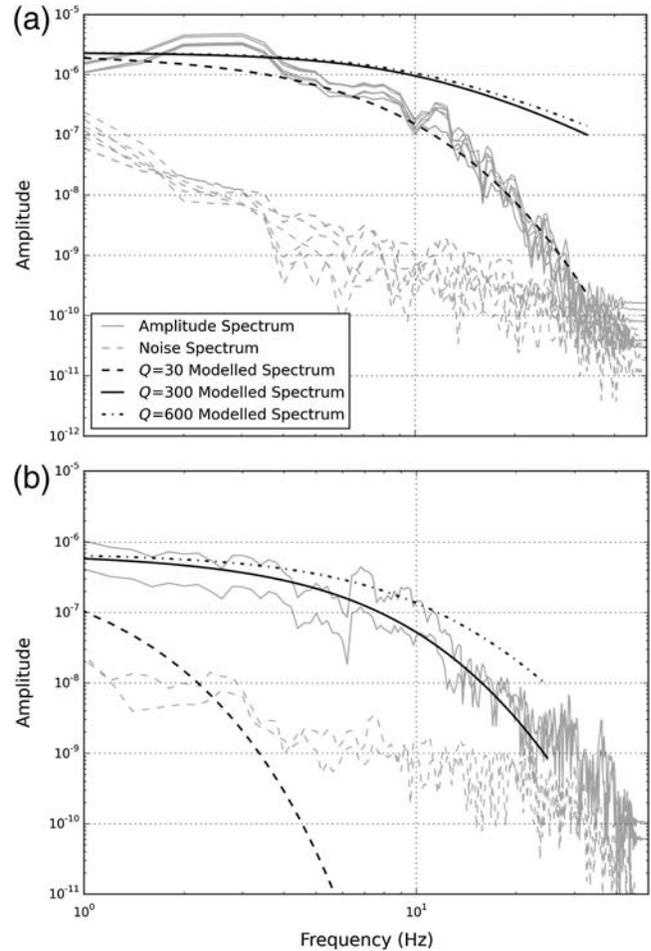
Figure 8. Source spectra for (a) six near and (b) two far events recorded on station NOLF. The gray curves show the observed displacement spectra, the gray dashed lines show the noise, and the black curves show the Brune model spectra using Q_S of 30, 300, and 600. The near events located at a distance of ~2 km and a depth of 0.9 km are best-fit with a Q of 30, the far events at a distance of 60 km and depth of 2.5 km are best-fit with a Q of 300.

$$\log(A_{ijk}) + 2 = M_{Lik} - a\log\left(\frac{r_{ij}}{17}\right) - b(r_{ij} - 17), \quad (14)$$

in which index i labels events, index j labels stations, and index k labels the component (north–south or east–west). Within the data, there is evidence of site effects; however, we choose to retain simplicity through excluding them from the inversion. This approach produces the New Ollerton (NOL) M_L scale

$$M_L = \log(A) + 1.17\log(r) + 0.0514r - 3.0, \quad (15)$$

which incorporates the Wood–Anderson gain correction and whose attenuation term (0.0514) is an order of magnitude larger than the current U.K. scale, which is 0.00183.

We use equation (9) to establish whether the inverted values for b are reasonable for the two scenarios (nearby
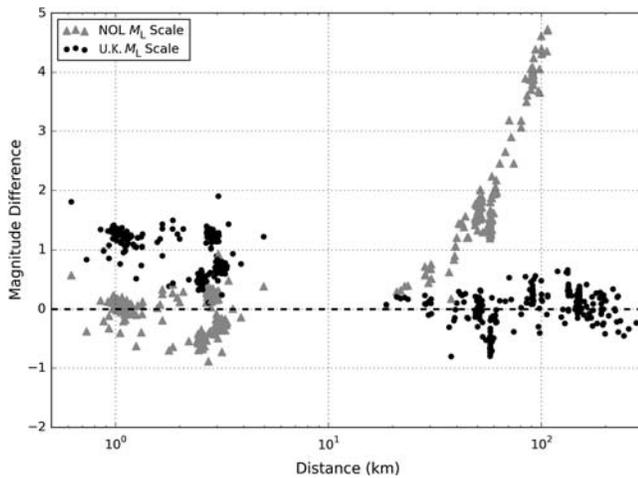
Figure 9. Magnitude differences for New Ollerton events observed on both NOL stations and the U.K. network. The NOL scale corrects the magnitudes at small hypocentral distances, but diverges significantly beyond the 17 km anchor point.
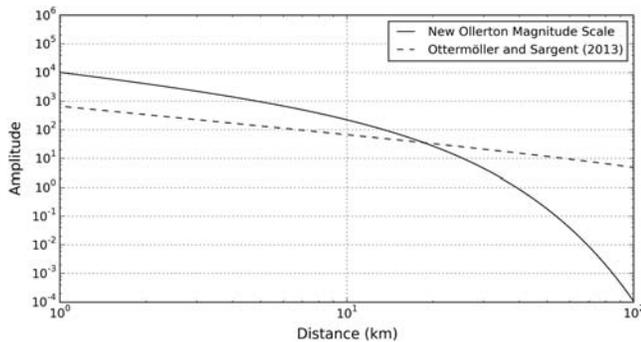
Figure 10. A comparison of the displacements anticipated for an M_L 1.0 event, as computed by the Ottemöller and Sargeant (2013) scale (dashed line) and that evaluated in equation (13). The scales converge at a hypocentral distance of 19 km, and at smaller distances the estimated ground displacements are different by an order of magnitude.

versus distant events). The value for b calculated by Ottemöller and Sargeant (2013) of 0.00183 can correspond to an S-wave velocity of 3.5 km/s and a Q of 200. The value for b calculated here (0.0514) would correspond to an S-wave velocity of 2 km/s and a Q of 35, and these are realistic values given the expected ray paths predominantly through the deeper crust and through the sediments, respectively.

Magnitude differences for events observed on both local and regional stations are presented in Figure 9. We determine the event magnitude through taking the mean M_L derived from the U.K. network and calculated using the U.K. M_L scale, and then produce differences for all available stations using the NOL and the U.K. M_L scales. The NOL scale successfully removes the discrepancy in the existing magnitude scale for nearby receivers, and converges with the U.K. scale at 19 km (Fig. 10). There is a lack of data in the 5–20 km
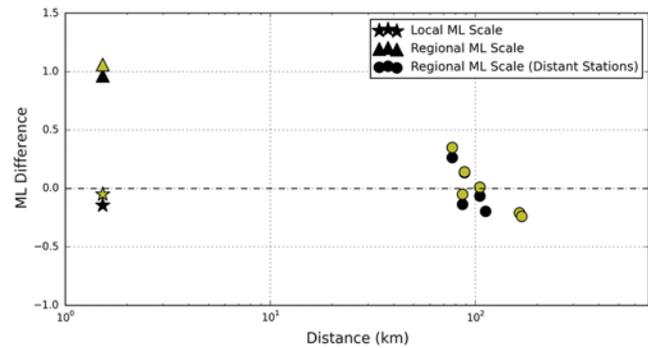
Figure 11. NOL scale (stars) applied to two Preese Hall events observed on the U.K. network, which significantly decreases the magnitude difference in contrast to the U.K. scale (triangles).

range, and after 19 km the NOL scale rapidly diverges and introduces large magnitude discrepancies.

Discussion

Although the New Ollerton dataset can be used to understand the impact that near-receiver events have on M_L scales, all the observations occur in a single location and over a narrow distance range. We therefore consider how appropriate the NOL scale is for different U.K. regions, and the valid distance range of the scale.

Sedimentary layers obviously vary in composition and depth (Kelly *et al.*, 2007; Nicolson *et al.*, 2014), which will influence the attenuation term b and the point at which the continental crust dominates the travel path. We consider the portability of the NOL scale through applying it to two Preese Hall events observed on both local stations and the U.K. network (Fig. 11). At Preese Hall, the NOL scale has significantly reduced the discrepancy between observed displacements at the nearby and distant stations (as identified in the Introduction) and is now consistent with the magnitude calculated on the U.K. network. Although in this case the NOL scale appears appropriate, if the geological composition of the shallow geology is significantly different, for example, limestone dominant, the attenuation term b may need to be recalibrated.

The depth of the sedimentary–continental interface will influence the crossover point between the NOL and U.K. scale. The distance range of 5–20 km is poorly represented in the New Ollerton dataset, and over this range the shift from a travel path dominated by the sedimentary layer to a path dominated by the continental crust occurs. There are uncertainties in the appropriateness of using a constant attenuation term over this range that cannot be addressed by this dataset, because both the apparent velocity and Q will be transitioning from sedimentary layer to continental crust values.

However, most of the U.K.'s shale gas activities are expected to take place across the north of England. Both the sites considered here (New Ollerton and Preese Hall) fall within the limits of the Bowland Shale as defined by the

BGS. The TLS will usually be administered using monitoring stations that are within 5 km of the proposed wells. We therefore suggest that the updated magnitude scale developed here is more suitable for the administration of the U.K.'s TLS than the U.K. standard M_L scale.

Conclusions

The U.K.'s hydraulic fracturing TLS will entail the deployment of monitoring stations in close proximity to well sites. However, the existing U.K. local magnitude scale is based on the observations of events at significant distances (>50 km) from receivers, and so is poorly calibrated for events recorded on nearby stations (<5 km). This discrepancy is significant because for nearby events the travel path is predominantly within the sedimentary layer, rather than the underlying basement, and so will require a different attenuation term in the M_L scale.

To address this issue, we studied the earthquakes recorded on a local monitoring network deployed to monitor coal-mining-induced seismicity at New Ollerton. Through consideration of apparent velocities, it can be observed that at distances greater than 10–15 km, the travel paths of recorded arrivals are predominantly through the continental crust because S-wave velocities stabilize at a value of $\sim$3.5 km/s. However, at closer distances, the apparent velocities reduce, implying a greater portion of the ray path is through the overlying sediments. A significant difference in Q estimates can also be seen between nearby events and distant events, with lower Q-values for nearby events implying greater attenuation through the sedimentary layers.

An updated local magnitude scale has been determined for nearby events using a least-squares inversion on the New Ollerton data, and we calculate that the attenuation term in the local magnitude scale should be increased from 0.00183 to 0.0514. This change reflects the slower, more attenuating nature of sedimentary layer in comparison with the continental crust. A further indication of the suitability of this scale is provided by the fact that it also removes the ground-motion discrepancies observed for the Preese Hall 2011 events at nearby stations. To ensure consistent local magnitude estimates during the future operation of the U.K.'s TLS, the updated magnitude scale should be used when local monitoring networks are within 5 km of the event epicenters.

Data and Resources

This study uses seismograms and amplitude measurements that were made by the British Geological Survey, which form part of the United Kingdom's seismic database. Mapping has been sourced from Digimap's Ordnance Survey collection (http://digimap.edina.ac.uk/, last accessed June 2016).

Acknowledgments

References

Abercrombie, R. E. (1995). Earthquake source scaling relationships from -1 to 5 M_L using seismograms recorded at 2.5-km depth, *J. Geophys. Res.* **100,** no. B12, 24,015–24,036.

Abercrombie, R. E. (1997). Near-surface attenuation and site effects from comparison of surface and deep borehole recordings, *Bull. Seismol. Soc. Am.* **87,** no. 3, 731–744.

Alsaker, A., L. B. Kvamme, R. A. Hansen, A. Dahle, and H. Bungum (1991). The M_L scale in Norway, *Bull. Seismol. Soc. Am.* **81,** no. 2, 379–398.

Atkinson, G. M., D. W. Greig, and E. Yenier (2014). Estimation of moment magnitude (M) for small events (M <4) on local networks, *Seismol. Res. Lett.* **85,** 1–19.

Best, A. I., J. Sothcott, and C. McCann (2007). A laboratory study of seismic velocity and attenuation anisotropy in near-surface sedimentary rocks, *Geophys. Prospect.* **55,** 609–625.

Bishop, I., P. Styles, and M. Allen (1993). Mining-induced seismicity in the Nottinghamshire coalfield, *Q. J. Eng. Geol. Hydrogeol.* **26,** no. 4, 253–279.

Booth, D. C. (2010). UK 1-D regional velocity models by analysis of variance of *P*-wave travel times from local earthquakes, *J. Seismol.* **14,** no. 2, 197–207.

Bott, M. H. P., R. E. Long, A. S. P. Green, A. H. J. Lewis, M. C. Sinha, and D. L. Stevenson (1985). Crustal structure south of the Iapetus suture beneath northern England, *Nature* **314,** no. 25, 724–727.

Brune, J. N. (1970). Tectonic stress and the spectra of seismic shear waves from earthquakes, *J. Geophys. Res.* **75,** 4997–5009.

Chadwick, R. A., and T. C. Pharaoh (1998). The seismic reflection Moho beneath the United Kingdom and adjacent areas, *Tectonophysics* **299,** no. 4, 255–279.

Clarke, H., L. Eisner, P. Styles, and P. Turner (2014). Felt seismicity associated with shale gas hydraulic fracturing: The first documented example in Europe, *Geophys. Res. Lett.* **41,** no. 23, 8308–8314.

Davis, M. W., N. J. White, K. F. Priestley, B. J. Baptie, and F. J. Tilmann (2012). Crustal structure of the British Isles and its epeirogenic consequences, *Geophys. J. Int.* **190,** no. 2, 705–725.

Department of Energy and Climate Change (2015). *Onshore Oil and Gas Exploration in the UK: Regulation and Best Practice*, Department of Energy and Climate Change, London, England.

Di Bona, M. (2016). A local magnitude scale for crustal earthquakes in Italy, *Bull. Seismol. Soc. Am.* **106,** no. 1, 242–258.

Eisner, L., E. Janská, I. Opršal, and P. Matoušek (2011). Seismic analysis of the events in the vicinity of the Preese Hall well, *Cuadrilla Resources Ltd., Final Rept.*

Havskov, J., and L. Ottemoller (2010). *Routine Data Processing in Earthquake Seismology: With Sample Data, Exercises and Software*, Springer, Dordrecht, The Netherlands.

Hutton, L. K., and D. M. Boore (1987). The M_L scale in southern California, *Bull. Seismol. Soc. Am.* **77,** no. 6, 2074–2094.

IMC Group Consulting Limited (2003). *Review of the Remaining Reserves at Deep Mines for The Department of Trade and Industry*, http://webarchive.nationalarchives.gov.uk/20060731065559/dti.gov.uk/files/file15982.pdf (last accessed December 2016).

Keir, D., G. W. Stuart, A. Jackson, and A. Ayele (2006). Local earthquake magnitude scale and seismicity rate for the Ethiopian rift, *Bull. Seismol. Soc. Am.* **96,** no. 6, 2221–2230.

Kelly, A., R. W. England, and P. K. H. Maguire (2007). A crustal seismic velocity model for the UK, Ireland and surrounding seas, *Geophys. J. Int.* **171,** no. 3, 1172–1184.

Langston, C. A., R. Brazier, A. A. Nyblade, and T. J. Owens (1998). Local magnitude scale and seismicity rate for Tanzania, East Africa, *Bull. Seismol. Soc. Am.* **88,** no. 3, 712–721.

Nicolson, H., A. Curtis, and B. Baptie (2014). Rayleigh wave tomography of the British Isles from ambient seismic noise, *Geophys. J. Int.* **198,** no. 2, 637–655.

O'Toole, T., J. P. Verdon, J. H. Woodhouse, and J. M. Kendall (2013). Induced seismicity at Preese Hall, UK—A review, *Proc. of the 75th European Association of Geoscientists and Engineers Conference and Exhibition 2013 Incorporating SPE EUROPEC 2013: Changing Frontiers,* 5369–5373.

Ottemöller, L., and S. Sargeant (2013). A local magnitude scale M_L for the United Kingdom, *Bull. Seismol. Soc. Am.* **103,** no. 5, 2884–2893.

Prejean, S. G., and W. L. Ellsworth (2001). Observation of earthquake source parameters at 2 km depth in the Long Valley Caldera, eastern California, *Bull. Seismol. Soc. Am.* **91,** no. 2, 165–177.

Prieto, G. A., R. L. Parker, and F. L. Vernon (2009). A Fortran 90 library for multitaper spectrum analysis, *Comput. Geosci.* **35,** no. 8, 1701–1710.

Richter, C. F. (1935). An instrumental earthquake magnitude scale, *Bull. Seismol. Soc. Am.* **25,** 1–32.

Scognamiglio, L., L. Margheriti, F. Mariano Mele, E. Tinti, A. Bono, P. De Gori, V. Lauciani, F. Pio Lucente, A. G. Mandiello, C. Marcocci, *et al.* (2012). The 2012 Pianura Padana Emiliana seismic sequence: Locations, moment tensors and magnitudes, *Ann. Geophys.* **55,** no. 4, 549–559.

Shearer, P. M. (2009). *Introduction to Seismology,* Cambridge University Press, Cambridge, Massachusetts.

Stork, A. L., and H. Ito (2004). Source parameter scaling for small earthquakes observed at the western Nagano 800-m-deep borehole, Central Japan, *Bull. Seismol. Soc. Am.* **94,** no. 5, 1781–1794.

Stork, A. L., J. P. Verdon, and J.-M. Kendall (2014). The robustness of seismic moment and magnitudes estimated using spectral analysis, *Geophys. Prospect.* **62,** no. 4, 862–878.

Tomlinson, J. P., P. Denton, P. K. H. Maguire, and D. C. Booth (2006). Analysis of the crustal velocity structure of the British Isles using teleseismic receiver functions, *Geophys. J. Int.* **167,** no. 1, 223–237.

Westaway, R. (2016). The importance of characterizing uncertainty in controversial geoscience applications: Induced seismicity associated with hydraulic fracturing for shale gas in northwest England, *Proc. Geol. Assoc.* **127,** no. 1, 1–17.

Wilson, M. P., R. J. Davies, G. R. Foulger, B. R. Julian, P. Styles, J. G. Gluyas, and S. Almond (2015). Anthropogenic earthquakes in the UK: A national baseline prior to shale exploitation, *Mar. Petrol. Geol.* **68,** 1–17.

School of Earth Sciences
University of Bristol
Wills Memorial Building, Queen's Road
Bristol BS8 1RJ, United Kingdom
antony.butcher@bristol.ac.uk
    (A.B., J.P.V., J.-M.K., J.W.)

British Geological Survey
Earthquake Seismology
The Lyell Centre
Edinburgh EH14 4AP, United Kingdom
    (R.L., B.B.)